Ultrafast Surface Imaging With an Increased Spatial Resolution Based on Polarization-Division Multiplexing

Fangjian Xing, Hongwei Chen, *Member, IEEE*, Shizhong Xie, *Senior Member, IEEE*, and Jianping Yao, *Fellow, IEEE, Fellow, OSA*

Abstract—Optical time stretch has been employed for ultrafast optical imaging based on space-to-wavelength-to-time mapping. However, temporal overlap between two adjacent time-stretched pulses is a disadvantageous factor that limits the spatial resolution, or the frame rate has to be reduced by reducing the pulse repetition rate to avoid the temporal overlap. To increase the spatial resolution without reducing the frame rate, we propose a novel technique based on polarization-division multiplexing, using a polarization modulator to generate two polarization interleaved pulse trains. Since two adjacent optical pulses are orthogonally polarized, the spacing between two adjacent pulses for one polarization direction is doubled, and the spatial resolution is doubled by using a dispersive element with two times the dispersion. The proposed approach is experimentally evaluated. An imaging system with an increased spatial resolution is demonstrated.

Index Terms—Optical time stretch, polarization division multiplexing, space-to-wavelength-to-time mapping, ultrafast imaging.

I. INTRODUCTION

NONDESTRUCTIVE imaging plays an important role in machine vision, which can find important applications in modern manufacturing, such as defect detection, quality control, dimensional metrology, numbering and surface examination [1]–[5]. Most of the inspections are now performed in a continuous real-time detection mode to realize quality evaluation of various materials or products, such as thin films, paper, concrete materials and silicon wafers [6]–[8]. In a conventional surface inspection system, a white line light source with a line scan camera is usually employed to scan the surface of a sample that is moved along the orthogonal direction [5], [8]. The scattered light from the surface is continuously detected by the line scan camera. However, the line scan rate of a conventional line detector is slow, restricted by the long response time of the detector used in the system, such as a charge-coupled device or complementary metal oxide semiconductor (CMOS) [9]. In pursuit of high temporal resolution, the detection sensitivity is sacrificed due to a short shutter time. The current highest frame rate of a CMOS image sensor is limited to a mega frames per second [10].

Recently, serial time-encoded amplified microscopy (STEAM) is demonstrated as a novel optical imaging technique that can achieve a high frame rate up to 10 MHz [11]–[14]. STEAM is an optical method that uses a combination of spatially and temporally dispersive elements with a broadband mode-lock laser source to achieve ultrafast single pixel imaging [15]–[20]. It should be noted that each single-shot pulse represents an image and the temporal overlap between adjacent pulses after time stretch must be avoided to ensure high imaging accuracy. For an optical pulse train from a mode-lock laser source having a line width of tens of nm and a repetition rate of tens of megahertz, the chromatic dispersion of a dispersive element used to perform wavelength-to-time mapping cannot be too large to avoid pulse overlap, which will limit the spatial resolution. In a photonic time-stretch system, to avoid temporal overlap, a solution is to use wavelength division multiplexing (WDM). A continuous-time large-bandwidth time-stretched signal is segmented and interleaved into multiple parallel channels based on virtual time gating (VTG), which makes the pulses in an individual channel have no temporal overlap [21], [22]. Base on this concept, a WDM microscopic imaging system with an increased resolution was proposed and demonstrated [23]. However, such a WDM technique has a limitation in producing a high quality image, since a bank of optical filters at different WDM bands are needed, which may not be designed to have ideal sharp edges to avoid interband interferences, thus affecting the spectrum at the boundary of the different WDM bands and reducing the quality of the image.

In this paper, we propose and experimentally demonstrate a polarization division multiplexing (PDM) time-stretch microscopic imaging system with nearly two-time increased spatial resolution without reducing the frame rate. The fundamental concept of the proposed approach is to use a polarization modulator (PolM) that is controlled by a square-wave sequence with an amplitude voltage of $V_\pi/2$, where V_π is the half-wave voltage of the PolM, from an arbitrary waveform generator (AWG) triggered by a synchronization signal from the mode-lock laser
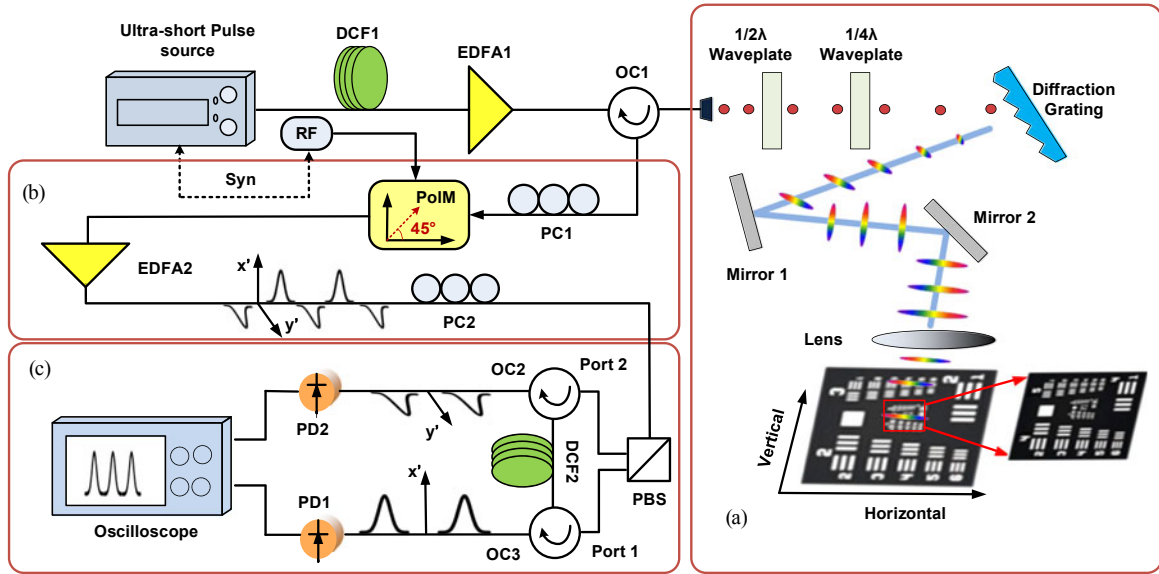
Fig. 1.   Schematic of the PMD time-stretch microscopic imaging system. (a) Free space optical path for wavelength-to-space mapping to encode the spatial information into the spectrum; (b) to convert the linearly polarized pulse train to two pulse trains with orthogonal polarizations. The PBS separates the two orthogonally polarized pulse trains into two channels; (c) the two pulse trains are sent to DCF2 to perform wavelength-to-time mapping. The time-stretched waveforms are captured by two PDs and digitized by a real-time oscilloscope. DCF: dispersion compensating fiber; EDFA: erbium doped fiber amplifier; OC: optical circulator; PC: polarization controller; PolM: polarization modulator; Syn: synchronization; RF: radio frequency; PBS: polarization beam splitter; PD: photodetector.

source, to alternatively change the polarization directions of adjacent pulses in the pulse train, to generate two interleaved pulse trains that are orthogonally polarized. Since two adjacent optical pulses are orthogonally polarized, the spacing between two adjacent pulses along one polarization direction is doubled, thus the spatial resolution is doubled due to the use of a dispersive element with doubled chromatic dispersion without reducing the frame rate. The proposed approach is experimentally evaluated. An imaging system with a spatial resolution of 18 μm and a beam width of 2.5 mm at a scan rate of 48.8 MHz is demonstrated. In the experiment, two samples including a resolution target and a silicon wafer are used. The improvement in image quality based on the proposed technique is experimentally verified.

II. PRINCIPLE

The schematic of the proposed PDM time-stretch microscopic imaging system is shown in Fig. 1. An ultra-short pulse train from a mode-lock laser source is sent to a dispersion compensating fiber (DCF1) to temporally stretch the pulses before the pulse train is sent to a diffraction grating via an erbium-doped fiber amplifier (EDFA1), a half-wave and a quarter-wave plate. The purpose to place DCF1 after the mode-lock laser source is to extend the pulse width to reduce the peak power to avoid damaging the later devices. However, since the system is a linear time-invariant system, it is identical to place DCF1 at a location just before photo-detection. The two wave plates are used to adjust the polarization direction of the light wave to the diffraction grating to achieve the highest diffraction efficiency due to the polarization dependence of the diffraction grating. At the output of the diffraction grating, a pulse is extended to a one-dimensional (1-D) beam due to the diffraction of the diffraction
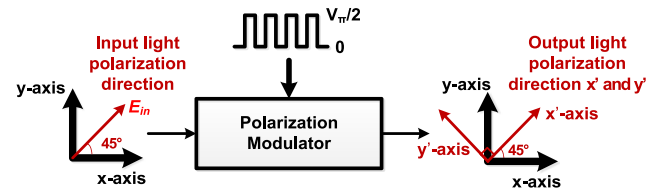

Fig. 2.   The principle of the PolM to generate two interleaved pulse trains that are orthogonally polarized. The light along the x'-axis comes out when the drive signal is 0 level. The light along the y'-axis comes out when the drive signal is $V_\pi/2$ level.

grating, which is sent via two mirrors and a focus lens to illuminate the sample. The sample is mounted on a translation stage that is moving perpendicular to the direction of the 1-D optical beam. The overall function of this free-space optics part, shown in Fig. 1(a) as Part 1, is to perform wavelength-to-space mapping to achieve 1-D imaging. The spatial information of the sample is encoded onto the spectrum of the pulse [24]. The entire two-dimensional (2-D) image of the sample is then captured by translating the sample along the vertical direction controlled by a stepper motor.

The second stage of this PDM time-stretch microscopic imaging system is to interleave the pulse train coming from Part 1, to form two pulse trains that are orthogonally polarized by using a PolM. The interleave operation is shown in Fig. 1(b). As can be seen, a linearly polarized pulse train from Part 1 is controlled by a polarization controller (PC1) to have an angle of 45° to one principal axis (*x*-axis in Fig. 2) of the PolM. The optical fields along the two principal axes are given by

$$\begin{bmatrix} E_x \\ E_y \end{bmatrix} = \begin{bmatrix} \cos\left(\frac{\pi}{4}\right) \\ \sin\left(\frac{\pi}{4}\right) \end{bmatrix} E_{\text{in}}, \tag{1}$$

where E_{in} is the optical filed of the light wave from Part 1, E_x and E_y are the optical fields along the two principal axes of the PolM. A square-wave sequence with an amplitude voltage of $V_\pi/2$ from an AWG triggered by a synchronization signal from the mode-lock laser source is applied to the PolM to alternatively change the polarization directions of the pulses in the pulse train, to generate two interleaved pulse trains that are orthogonally polarized. The optical field at the output of the PolM can be expressed as [25]

$$\begin{bmatrix} E_{x'} \\ E_{y'} \end{bmatrix} = \begin{bmatrix} \frac{\sqrt{2}}{2} & \frac{\sqrt{2}}{2} \\ -\frac{\sqrt{2}}{2} & \frac{\sqrt{2}}{2} \end{bmatrix} \begin{bmatrix} E_x \exp\left[j\pi\left(\frac{v_{\text{RF}}}{V_\pi}\right)\right] \\ E_y \exp\left[-j\pi\left(\frac{v_{\text{RF}}}{V_\pi}\right)\right] \end{bmatrix}, \quad (2)$$

where v_{RF} is the voltage applied to the PolM, $E_{x'}$ is the optical component along the x'-axis and $E_{y'}$ is the optical component along the y'-axis, as shown in Fig. 2. When the voltage of the square-wave sequence is $v_{\text{RF}} = 0$, the polarization direction of the linearly polarized pulse is not changed, which is along the x'-axis. On the other hand, when the voltage of the square-wave is $v_{\text{RF}} = V_\pi/2$, the polarization direction of the linearly polarized pulse is rotated by 90°, which is along the y'-axis. By using a polarization beam splitter (PBS) with its principal axes aligned with the two orthogonal polarization directions of the two pulse trains, realized by tuning PC2, the two orthogonally polarized pulse trains are separated (demultiplexed) physically.

The physically separated polarization-interleaved pulse trains are sent to a second DCF (DCF2) from the other sides, to perform wavelength-to-time mapping, to convert the sample information encoded on the pulse spectrums to the amplitudes of two temporal waveforms, as shown in Fig. 1(c). A second EDFA (EDFA2) is used to further compensate for the insertion loss. Thus, two time-stretched pulse trains carrying the imaging information in the time domain are obtained, which are detected by two photodetectors (PD1 and PD2), sampled by a high-speed oscilloscope, and reconstructed off-line using a digital signal processor. Since the repetition rate of the two pulse trains is half than that of the original pulse train, the dispersion of the dispersive element can be doubled, thus the spatial resolution is increased by nearly two times while maintaining the same frame rate without pulse overlapping. Note that spatial resolution is improved since the proposed system is temporal-dispersion limited, the use of a dispersive element with a higher value of dispersion can further stretch the pulses in the pulse train without causing pulse overlap, making the spectral resolution increased. It should also be noted, however, a higher value of dispersion will usually bring more loss and thus a higher gain is needed to compensate for the loss. In the system, this is done by using the two EDFAs.

III. EXPERIMENT

An experiment based on the setup shown in Fig. 1 is carried out. The optical pulse train used for imaging is generated from a passively mode-locked laser source (IMRA femtolite 780) with a center wavelength of 1558 nm, a 10-dB bandwidth of ~14 nm, and a pulse repetition rate of 48.8 MHz. The spectrum of a pulse from the pulse train is shown in Fig. 3(a). The pulse
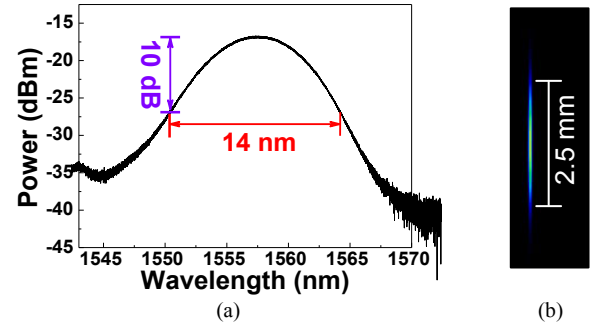

Fig. 3. (a) The spectrum of an optical pulse from the mode-lock laser, and (b) the image of the 1-D rainbow beam at the output of the focus lens.

train from the mode-lock laser source is sent to DCF1 with a value of dispersion of −948 ps/nm to temporally stretch the pulse, which is then amplified by EDFA1. The loss of DCF1 is about 7 dB. Note that the use of DCF1 just after the mode-lock laser source is to broaden the pulse to reduce the peak power of the pulse train to avoid damaging the PolM and other components. However, the function is identical to placing DCF1 at any place in the system since the system is a linear time-invariant system. The time-stretched pulse train is sent to the diffraction grating to perform wavelength-to-space mapping. The diffraction grating has a groove density of 1200 lines/mm. A one-dimension spatially dispersed pulse is obtained at the output of the diffraction grating. A singlet spherical lens with a focal length of 100 mm is then used to focus the dispersed pulse to be a rainbow line. The focused rainbow line is incident onto a sample that is placed at the focal plane of the lens. The 1-D rainbow line is measured by a beam profiler (Thorlabs: BP209IR/M) which is shown in Fig. 3(b). The rainbow line has a width of 20 μm and a length of 2.5 mm. Consequently, when the sample is illuminated by the optical pulse, its reflection from the sample at different wavelengths in a range of 1551–1565 nm corresponds to a different spatial coordinate along the horizontal direction. The optical power illuminated on sample is around 5 dBm. Thus, the information of the sample is encoded on the spectrum of the rainbow pulse, which is reflected back and directed via an optical circulator (OC) and a PC (PC1) to the PolM. The optical power at port 3 of the OC is measured to be about 0 dBm. A square-wave sequence with an amplitude voltage of $V_\pi/2$ from the AWG triggered by a synchronization signal from the mode-lock laser source is applied to the PolM to alternatively change the polarization directions of adjacent pulses in the pulse train, to generate two orthogonally polarized pulse trains. The PolM (Versawave) has a bandwidth of 40 GHz, and a half-wave voltage of 3.5 V. The polarization extinction ratio of the PolM is about 20 dB. A radio frequency power amplifier is used to amplify the square-wave sequence to have an amplitude voltage of $V_\pi/2$. The polarization directions of the two orthogonally polarized pulse trains are aligned with the principal axes of the PBS by tuning PC2, to physically separate the two pulse trains. Here the optical power is about 6 dBm. Fig. 4(a) shows the two interleaved optical pulse trains at the outputs of the PBS. The repetition period (41.1 ns) of
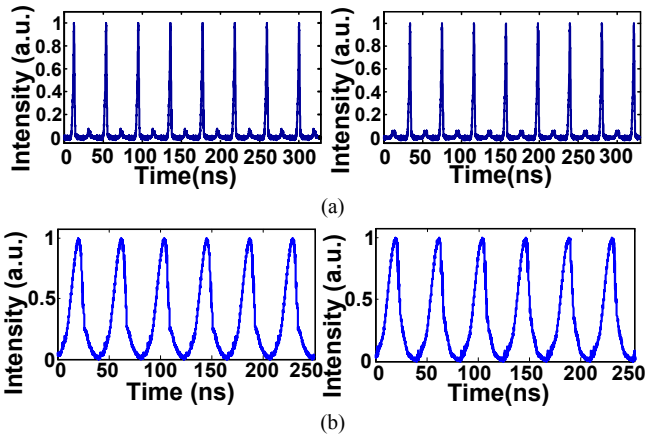
Fig. 4. The two polarization-interleaved optical pulse trains at the output of the PBS. (a) The waveforms that are temporally stretched by DCF1 with a value of dispersion of −948 ps/nm; (b) the waveforms that are temporally stretched by both DCF1 and DCF2 with a total value of dispersion of ∼−2.7 ns/nm.
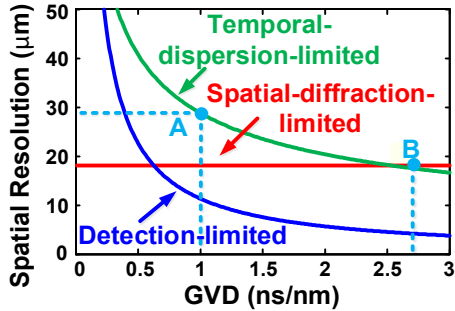

Fig. 5. Theoretical spatial resolution of the ultrafast line scan imaging system for three limiting cases: spatial-diffraction limited (red), temporal-dispersion limited (green), and detection limited (blue). The position of spot A denotes the final resolution of the system with a value of dispersion of ∼−1 ns/nm is limited by temporal dispersion. The position of spot B denotes the final resolution of the system with a value of dispersion of ∼−2.7 ns/nm is limited by spatial diffraction. The system parameters: the center wavelength is 1558 nm, the input beam waist is 8.5 mm, the focal length of the spherical lens is 100 mm, the diffraction grating period is 1/1200 mm, and the detection bandwidth is 7 GHz.

the pulse trains is two times the period of the original pulse train. Then, the two pulse trains are sent to DCF2 with a value of dispersion of ∼−1.7 ns/nm from the other sides, to perform the wavelength-to-time mapping (in fact, DCF1 and DCF2 are working together to perform the wavelength-to-time mapping), to convert the information encoded on the spectrum to the time domain. The loss of DCF2 is about 8 dB. Note that the residual pulses are also amplified by EDFA1, but they are very weak. The total optical gain of the two EDFAs is ∼35 dB and the spectrum of the pulses in the pulse train is within the gain bandwidth of the EDFAs. Fig. 4(b) shows the waveforms of the orthogonally polarized pulse trains after time stretch by DCF1 and DCF2. The residual pulses disappear after passing through DCF2. The temporarily stretched pulse trains, each having a power of −5 dBm, are detected by two high-speed PDs, and digitized by a high-speed oscilloscope (Tektronix TDS7704B) with a bandwidth of 7 GHz and a sampling rate of 20 Gs/s.

The spatial resolution of a line scan imaging system based on the space-to-wavelength-to-time mapping is limited by: 1) the spatial diffraction limited resolution, 2) the spectral resolution of the dispersive fiber defined by the stationary-phase approximation, and 3) the temporal resolution of the optical detection system including the PDs and the back-end digitizer [26], [27]. The contributions of the three factors to the actual spatial resolution of our proposed imaging system are evaluated and are shown in Fig. 5. The values of the parameters used are the same as the ones used in our experiment, which are given in the figure caption of Fig. 5. For our used mode-lock laser source with a pulse period of ∼20 ns, a section of DCF (DCF1) with a value of dispersion of ∼−1 ns/nm is employed for time stretch, and the pulse train after time stretch has no temporal overlap. In this case (called as Case 1), the spatial resolution is restricted by factor 2, corresponding to a resolution of ∼28 μm (marked by letter A in Fig. 5). When using the PDM technique, the total value of dispersion is increased up to ∼−2.7 ns/nm (DCF1+DCF2). For this case (called as Case 2), the resolution is attributed to the spatial diffraction which is ∼18 μm (marked by letter B in Fig. 5), and the total line scan rate is still maintained at 48.8 MHz. Here we should point out that it is not necessary to increase the dispersion to excess the value of ∼−2.7 ns/nm, since the final resolution is always limited by factor 1.

To evaluate the performance of the proposed imaging system, we first perform optical imaging of a USAF-1951 standard resolution target under two different values of dispersion of ∼−1 ns/nm and ∼−2.7 ns/nm. As a proof-of-concept demonstration, the imaging system works in the single-shot line scan mode, along the scan direction shown in Fig. 1(a) at a frame rate of 48.8 MHz. The 2-D imaging is achieved by moving the sample in the vertical direction. Fig. 6(a)–(c) shows the three 2-D images of the resolution target: the image obtained from a bright-field microscope, the image obtained for Case 1 with a value of dispersion of ∼−1 ns/nm and the image obtained for Case 2 with a value of dispersion of ∼−2.7 ns/nm. Here the imaging region covers the group 4 elements from 2 to 6, as shown in Fig. 6(a). For group 4 elements from 6 to 2, the line widths are from 17.5 to 28 μm. It is clear that the image formed using a DCF with larger dispersion results in better image quality in terms of spatial resolution. The experimental results in Fig. 6(b) and (c) have confirmed the effectiveness of the proposed technique to increase the spatial resolution. It should be noted that both images are reconstructed from raw data without any additional data processing. The difference in quality is only resulted from the imaging system, where different values of dispersion are employed, leading to different spatial resolution. Though the system is diffraction limited, the quality of Fig. 6(c) is more blurred than that of Fig. 6(a) because of its poor resolution.

To demonstrate the proposed system for general applications, the imaging of a silicon chip is then performed. This silicon chip contains waveguides with different sizes and shapes. For Case 1 where the DCF for time stretch has a value of dispersion of ∼−1 ns/nm, the fine structures etched onto the chip are hardly visible, as shown in the dashed-red circle of Fig. 7(b), compared
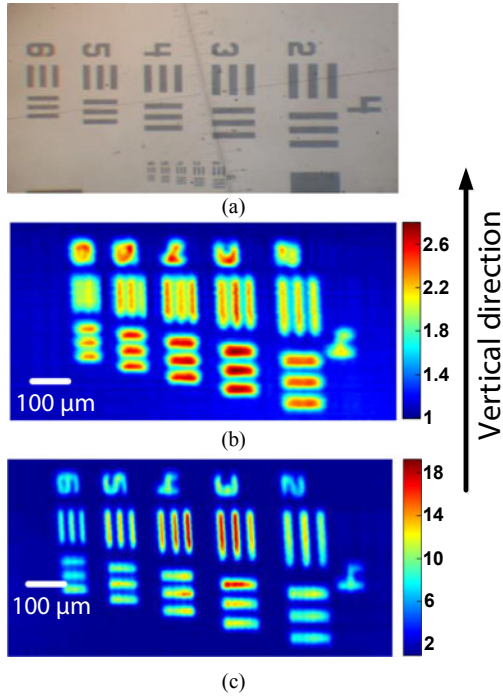
Fig. 6. Surface imaging of a standard resolution target (USAF-1951). (a) The bright-field microscopic image of the group 4 elements from 2 to 6 of the resolution target; (b) 2-D image obtained for Case 1 when the value of dispersion is ~−1 ns/nm; (c) 2-D image obtained for Case 2 when the value of dispersion is ~−2.7 ns/nm.

with the bright-field microscope image shown in the dashed-red circle of Fig. 7(a). In contrast, the 2-D image obtained based on the proposed technique using a DCF with a value of dispersion of ~−2.7 ns/nm shows a greatly improved image quality. The fine line waveguides, shown in the dashed-red circle of Fig. 7(c), can be well distinguished. In addition, for the part of the image in the dashed-red box, the details of the micro-square for Case 2 are also clearer than that for Case 1. The results in Fig. 7 have further proved the improvement in spatial resolution using the proposed imaging system without sacrificing the frame rate.

A nearly doubled spatial resolution is confirmed by the experiment. In the experiment, the value of chromatic dispersion of the DCF for wavelength-to-time mapping device is ~−2.7 ns/nm. Based on the PDM technique, the scan rate maintains constant while the value of dispersion is increased from ~−1 ns/nm to ~−2.7 ns/nm, corresponding to a spatial resolution change from 28 to 18 μm. Unlike the VTG technique, each single-shot line scan image is no longer carved into multiple channels to avoid temporal overlap. With no separation of each image-encoded pulse, the final 2-D images can be reconstructed from the raw data without further data processing and the imaging quality is greatly improved. Note that the imaging system demonstrated here is dispersion limited. Thus, the use of a dispersive element with a higher value of dispersion can increase the spatial resolution. For an imaging system that is diffraction limited [28], the scan rate can be increased until the system becomes dispersion limited. Then, the PDM technique can be employed to further improve the spatial resolution.
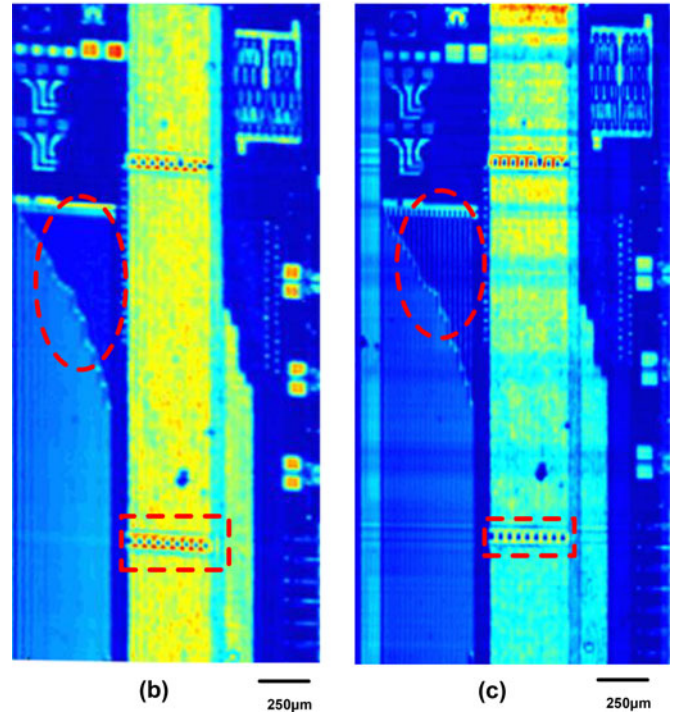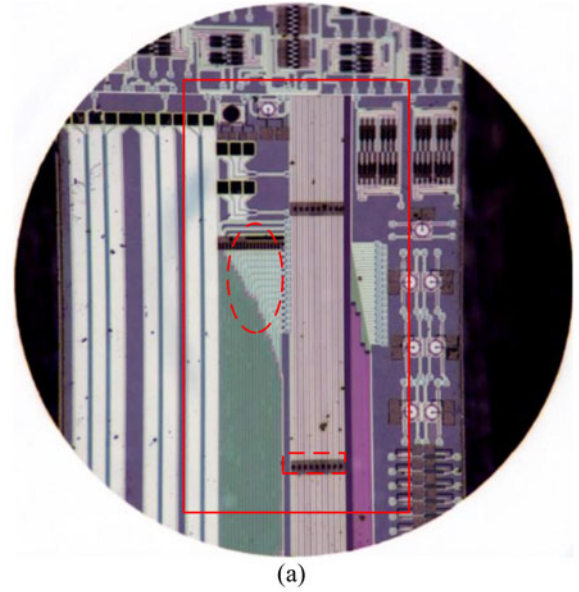

Fig. 7. Surface imaging of a silicon chip. (a) The bright-field microscopic image of the silicon chip; (b) 2-D image obtained for Case 1 when the value of dispersion is ~−1 ns/nm; (c) 2-D image obtained for Case 2 when the value of dispersion is ~−2.7 ns/nm.

IV. CONCLUSION

We have proposed and experimentally demonstrated a novel time-stretch imaging system based on PDM technique with increased spatial resolution without reducing the frame rate. The fundamental concept of the proposed approach was to use a PolM to make the pulse train from a mode-lock laser source into two interleaved pulse trains with orthogonal polarizations. Since the spacing between two adjacent pulses in a new pulse train

for one polarization direction is doubled, the value of dispersion of the dispersive element in the system for wavelength-to-time mapping could be doubled without introducing pulse overlap. Thus, the spatial resolution was doubled while maintaining the same frame rate. The proposed technique was experimentally demonstrated. In the experiment, two samples, one was a standard resolution target and the other was a silicon chip, were used. For a DCF with a higher value of dispersion, the image quality is increased. The results have confirmed the effectiveness of the proposed approach for resolution-improved imaging.

REFERENCES

[1] Y. F. Zhang and R. R. Bressee, "Fabric effect detection and classification using image analysis," *Tex. Res. J.*, vol. 65, no. 1, pp. 1–9, Jan. 1995.
[2] A. Kumar, "Computer-vision-based fabric defect detection: A survey," *IEEE Trans. Ind. Electron.*, vol. 55, no. 1, pp. 348–363, Jan. 2008.
[3] R. Rösch, F. C. Krebs, D. M. Tanenbaum, and H. Hoppe, "Quality control of roll-to-roll processed polymer solar modules by complementary imaging methods," *Sol. Energy Mater. Sol. Cells*, vol. 97, pp. 176–180, Feb. 2012.
[4] R. Leach, *Optical Measurement of Surface Topography*. Berlin, Germany: Springer-Verlag, 2011.
[5] B. C. Leslie, M. Nikoonahad, and K. B. Wells, "Optical scanning system for surface inspection," U.S. Patent 6 081 325, Jun. 27, 2000.
[6] T. Mäenpää, M. Turtinen, and M. Pietikäinen, "Real-time surface inspection by texture," *Real-Time Imag.*, vol. 9, no. 5, pp. 289–296, Oct. 2003.
[7] S. Cubero, N. Aleixos, E. Moltó, J. Gómez-Sanchis, and J. Blasco, "Advances in machine vision applications for automatic inspection and quality evaluation of fruits and vegetables," *Food Bioprocess Technol.*, vol. 4, no. 4, pp. 487–504, Jul. 2011.
[8] J. S. Batchelder, "Semiconductor wafer surface inspection apparatus and method," U.S. Patent 4 740 708, Apr. 26, 1988.
[9] J. Fürtler, E. Bodenstorfer, M. Rubik, K. J. Mayer, J. Brodersen, and C. Eckel, *High-Performance Smart Cameras*. New York, NY, USA: Springer, 2010, pp. 119–135.
[10] G. Bub, N. Nebeker, and R. Light, "New approaches for high-speed, high-resolution imaging," in *Novel Advances in Microsystems Technologies and Their Applications*. New York, NY, USA: Taylor & Francis, 2013, pp. 149–159.
[11] K. Goda, K. K. Tsia, and B. Jalali, "Amplified dispersive Fourier-transform imaging for ultrafast displacement sensing and barcode reading," *Appl. Phys. Lett.*, vol. 93, no. 13, p. 131109, Sep. 2008.
[12] K. Goda, K. K. Tsia, and B. Jalali, "Serial time-encoded amplified imaging for real-time observation of fast dynamic phenomena," *Nature*, vol. 458, pp. 1145–1149, Apr. 2009.
[13] F. Qian, Q. Song, E. K. Tien, S. K. Kalyoncu, and O. Boyraz, "Real-time optical imaging and tracking of micron-sized particles," *Opt. Commun.*, vol. 282, no. 24, pp. 4672–4675, Dec. 2009.
[14] H. Chen, C. Lei, F. Xing, Z. Weng, M. Chen, S. Yang, and S. Xie, "Multiwavelength time-stretch imaging system," *Opt. Lett.*, vol. 39, no. 7, pp. 2202–2205, Apr. 2014.
[15] C. Zhang, Y. Qiu, R. Zhu, K. K. Wong, and K. K. Tsia, "Serial time-encoded amplified microscopy (STEAM) based on a stabilized picosecond supercontinuum source," *Opt. Exp.*, vol. 19, no. 17, pp. 15810–15816, Aug. 2011.
[16] T. T. Wong, A. K. Lau, K. K. Wong, and K. K. Tsia, "Optical time-stretch confocal microscopy at 1 μm," *Opt. Lett.*, vol. 37, no. 16, pp. 3330–3332, Oct. 2012.
[17] Y. Qiu, J. Xu, K. K. Wong, and K. K. Tsia, "Exploiting few mode-fibers for optical time-stretch confocal microscopy in the short near-infrared window," *Opt. Exp.*, vol. 20, no. 22, pp. 24115–24123, Oct. 2012.
[18] F. Xing, H. Chen, M. Chen, S. Yang, and S. Xie, "Simple approach for fast real-time line scan microscopic imaging," *Appl. Opt.*, vol. 52, no. 28, pp. 7049–7053, Oct. 2013.
[19] T. T. Wong, A. K. Lau, K. K. Ho, M. Y. Tang, J. D. Robles, X. Wei, A. C. Chan, A. H. Tang, E. Y. Lam, K. K. Wong, G. C. Chan, H. C. Shum, and K. K. Tsia, "Asymmetric-detection time-stretch optical microscopy (ATOM) for ultrafast high-contrast cellular imaging in flow," *Sci. Rep.*, vol. 4, art. no. 3656, pp. 2045–2322, Jan. 2014.
[20] F. Xing, H. Chen, M. Chen, S. Yang, and S. Xie, "World's fastest real-time line scan microscopic imaging system with 1 GHz frame rate," presented at the IEEE Conf. Lasers Electro-Opt. Pacific Rim, Kyoto, Japan, 2013.
[21] Y. Han and B. Jalali, "Continuous-time time-stretched analog-to-digital converter array implemented using virtual time gating," *IEEE Trans. Circuits Syst. I, Reg. Papers*, vol. 52, no. 8, pp. 1502–1507, Aug. 2005.
[22] J. H. Wong, H. Q. Lam, R. M. Li, K. E. K. Lee, V. Wong, P. H. Lim, S. Aditya, P. P. Shum, S. H. Xu, K. Wu, and C. Ouyang, "Photonic time-stretched analog-to-digital converter amenable to continuous-time operation based on polarization modulation with balanced detection scheme," *J. Lightw. Technol.*, vol. 29, no. 20, pp. 3099–3106, Oct. 2011.
[23] F. Xing, H. Chen, C. Lei, Z. Weng, M. Chen, S. Yang, and S. Xie, "Serial wavelength division 1 GHz line-scan microscopic imaging," *Photon. Res.*, vol. 2, no. 4, pp. B31–B34, Aug. 2014.
[24] G. J. Tearney, R. H. Webb, and B. E. Bouma, "Spectrally encoded confocal microscopy," *Opt. Lett.*, vol. 23, no. 15, pp. 1152–1154, Aug. 1998.
[25] J. D. Bull, N. A. F. Jaeger, H. Kato, M. Fairburn, A. Reid, and P. Ghanipour, "40-GHz electro-optic polarization modulator for fiber optic communications systems," *Proc. SPIE*, vol. 5577, pp. 133–143, Sep. 2004.
[26] K. Goda, D. R. Solli, K. K. Tsia, and B. Jalali, "Theory of amplified dispersive Fourier transformation," *Phys. Rev. A*, vol. 80, no. 4, p. 043821, Oct. 2009.
[27] K. K. Tsia, K. Goda, D. Capewell, and B. Jalali, "Performance of serial time-encoded amplified microscopy," *Opt. Exp.*, vol. 18, no. 10, pp. 10016–10028, May 2010.
[28] X. Wei, A. K. S. Lau, T. T. W. Wong, C. Zhang, K. K. Tsia, and K. K. Y. Wong, "Coherent laser source for high frame-rate optical time-stretch microscopy at 1.0 μm," *IEEE J. Sel. Topics Quantum Electron.*, vol. 20, no. 5, pp. 1100306–1100306, Sep. 2014.

Fangjian Xing received the B. E. degree in optical information science and technology from the Harbin Institute of Technology, Harbin, China, in 2010. He is currently working toward the Ph.D. degree in electronic engineering at the Department of Electronic Engineering, Tsinghua University, Beijing, China.

From May 2014 to October 2014, he was an exchange Student with the Microwave Photonics Research Laboratory, School of Electrical Engineering and Computer Science, University of Ottawa, Ottawa, ON, Canada. His current research interests include ultrafast optical imaging and signal processing.

Hongwei Chen (M'07) received the B.E. and Ph.D. degrees in electronic engineering from Tsinghua University, Beijing, China, in 2001 and 2006, respectively.

He is currently with the Faculty of the Department of Electronic Engineering, Tsinghua University. His current research interests include radio-over-fiber techniques, high-speed optical communications, optical packet-switching networks, and ultrafast optical image technique.

Dr. Chen received the Best Student Paper Award at the Asia-Pacific Optical Communications (APOC) in 2004, where he was a subcommittee Member in 2005, 2007, and 2008, and also at the Pacific Rim Conference on Lasers and Electro-Optics in 2007.

Shizhong Xie (M'94–SM'98) received the Graduation degree in 1970 and the M.S. degree in electronic engineering from Tsinghua University, Beijing, China, in 1981.

From 1987 to 1988, he was a Visiting Scholar with the University of Southern California, Los Angeles, CA, USA. In 1989, he was a Senior Visitor holding a Royal Society British Telecom Fellowship at the University College London, London, U.K. From 1970 to 1978, he was with the Faculty of the Department of Electronic Engineering, Tsinghua University, where since 1981, he has been a Full Professor and the Director of Optical Communication Research Institute. He has led or participated in many major government-funded research programs in the area of optical network, including China Advance Info-Optical Network, the National Science Foundation of China Network, and the National High-Performance Broadband Information Network, where he was a Member of the expert groups steering those programs. His current research interests include dense-wavelength-division multiplexing optical fiber communications, broadband optical networks, optical packet switching, UV-induced fiber Bragg gratings, holey fibers, their application in optical fiber communications, and ultrafast optical imaging He is a Senior Member of the IEEE Photonics Society, the Chinese Institute of Electronics, and the Chinese Optical Society.

Jianping Yao (M'99–SM'01–F'12) received the Ph.D. degree in electrical engineering from the Université de Toulon, Toulon, France, in December 1997.

In 1998, he joined the School of Electrical and Electronic Engineering, Nanyang Technological University, Singapore, as an Assistant Professor. In December 2001, he joined the School of Electrical Engineering and Computer Science, University of Ottawa, Ottawa, ON, Canada, as an Assistant Professor, where he became an Associate Professor in 2003 and a Full Professor in 2006. In 2007, he was appointed as the University Research Chair in Microwave Photonics. From July 2007 to June 2010, he was the Director of the Ottawa-Carleton Institute for Electrical and Computer Engineering, where he was again reappointed as the Director in 2013. He is currently a Professor and the University Research Chair at the School of Electrical Engineering and Computer Science, University of Ottawa. He has published more than 450 papers, including more than 260 papers in peer-reviewed journals and 190 papers in conference proceedings. He was a Guest Editor for the Focus Issue *on Microwave Photonics in Optics Express* in 2013 and a Feature Issue on Microwave Photonics in *Photonics Research* in 2014. He is currently a Topical Editor for *Optics Letters*, and serves on the Editorial Board of the IEEE TRANSACTIONS ON MICROWAVE THEORY AND TECHNIQUES. He is the Chair of numerous international conferences, symposia, and workshops, including the Vice-TPC Chair of the 2007 IEEE *Microwave Photonics Conference*, TPC Co-Chair of the 2009 and 2010 Asia-Pacific Microwave Photonics Conferences, TPC Chair of the high-speed and broadband wireless technologies subcommittee of the 2009–2012 IEEE *Radio Wireless Symposia*, TPC Chair of the microwave photonics subcommittee of the 2009 IEEE *Photonics Society Annual Meeting*, TPC Chair of the 2010 IEEE *Microwave Photonics Conference*, and General Co-Chair of the 2011 IEEE *Microwave Photonics Conference*.

Dr. Yao is a Registered Professional Engineer of Ontario. He is a Fellow of the Optical Society of America and the Canadian Academy of Engineering. He received the International Creative Research Award at the University of Ottawa in 2015 and the George S. Glinski Award for Excellence in Research in 2007. He was selected for receiving an inaugural OSA outstanding reviewer award in 2012. He is an IEEE MTT-S Distinguished Microwave Lecturer from 2013 to 2015.